Phys. Lett. B 855 (2024) 138770

Contents lists available at ScienceDirect

Physics Letters B

journal homepage: www.elsevier.com/locate/physletb

Letter

Strong coupling effects on near-barrier $^{15}C + {}^{208}Pb$ elastic scattering

V.G. Távora [a], J.D. Ovejas [a], I. Martel [b,*], N. Keeley [c], L. Acosta [a,d], M.J.G. Borge [a], O. Tengblad [a], A.A. Arokiaraj [e], M. Babo [e], J. Cederkall [f], N. Ceylan [b], A. Di Pietro [g], J.P. Fernández-García [g,h], P. Figuera [g], L.M. Fraile [i], H.O.U. Fynbo [j], D. Galaviz [k], C. García-Ramos [b], R. Honório [k], J.H. Jensen [j], B. Jonson [l], K.W. Kemper [m], A. Knyazev [f], R. Kotak [n], T. Kurtukian-Nieto [a], M. Madurga [o], G. Marquínez-Durán [b], M. Munch [j], A.K. Orduz [p], J. Park [f], L. Peralta [k], A. Perea [a], T. Pérez-Alvarez [b], R. Raabe [e], M. Renaud [e], K. Riisager [j], K. Rusek [q], A.M. Sánchez-Benítez [r], J. Sánchez-Segovia [b], P. Teubig [k], S. Viñals [a], M. Wolińska-Cichocka [q], R. Wolski [s], J. Yang [e]

[a] Instituto de Estructura de la Materia, CSIC, Madrid, Spain
[b] Science and Technology Research Centre, University of Huelva, Spain
[c] National Centre for Nuclear Research, Otwock, Poland
[d] Instituto de Fí sica, Universidad Nacional Autónoma de Mexico, Mexico
[e] Instituut voor Kern-en Stralingsfysica, KU Leuven, Belgium
[f] Physics Department, Lund University, Sweden
[g] INFN, Laboratori Nazionali del Sud, Catania, Italy
[h] Departamento de FAMN, Universidad de Sevilla, Apartado 1065, 41080 Sevilla, Spain
[i] Grupo de Física Nuclear, IPARCOS, EMFTEL, Universidad Complutense de Madrid, Spain
[j] Department of Physics and Astronomy, University of Aarhus, Denmark
[k] LIP - Laboratory for Instrumentation and Experimental Particle Physics, Lisbon, Portugal
[l] Department of Physics, Chalmers University of Technology, Göteborg, Sweden
[m] Department of Physics, The Florida State University, Tallahassee, FL, USA
[n] Astrophysics Research Centre, Queen's University Belfast, UK
[o] Department of Physics and Astronomy, University of Tennessee, Knoxville, USA
[p] Grand Accélérateur National d'Ions Lourds, Caen, France
[q] Heavy Ion Laboratory, University of Warsaw, Poland
[r] Centro de Estudios Avanzados en Física, Matemáticas y Computación, University of Huelva, Spain
[s] ul. Ugorek 16/43, 31-456 Kraków, Poland

ARTICLE INFO

Editor: B. Blank

Keywords:
Direct nuclear reactions
Radioactive beams
Elastic scattering
Optical model
Coupled channels

ABSTRACT

The presence of a neutron halo in ^{15}C has been demonstrated in several reaction experiments at intermediate energies. In the present study, the dynamical effects of this structure are observed for the first time at Coulomb barrier energies in the $^{15}C + {}^{208}Pb$ quasi-elastic scattering at $E_{lab} = 65$ MeV, measured at the HIE-ISOLDE facility, CERN using the high-granularity detector array GLORIA. A combined continuum discretised coupled channels and coupled reaction channels calculation describes the data well and significant coupling effects due both to breakup and single-neutron stripping are identified.

1. Introduction

A number of light, neutron-rich nuclides with low $1n$ or $2n$ separation energies such as ^{6}He, ^{11}Li, ^{11}Be or ^{14}Be exhibit the extended neutron distributions that give rise to the so-called neutron halo [1,2]. At collision energies around the Coulomb barrier, the nuclear reaction dynamics of systems involving these nuclei are dominated by strong coupling between the elastic scattering, breakup, transfer, and fusion

* Corresponding author.
E-mail addresses: imartel@uhu.es (I. Martel), mm.munch@gmail.com (M. Munch).

https://doi.org/10.1016/j.physletb.2024.138770
Received 2 February 2024; Received in revised form 15 May 2024; Accepted 30 May 2024
Available online 4 June 2024

channels. This leads to phenomena not usually present in the scattering of other, non-halo isotopes (see, e.g., Ref. [3] for a recent review): absence of a Coulomb rainbow peak, long range reaction mechanisms, large cross sections for breakup and neutron stripping reactions, and the dynamical decoupling of the core from the halo neutrons, among others. In particular, the weak binding energy and extended density distribution of halo neutrons imply an important coupling effect on the near-barrier elastic scattering due to breakup and/or neutron stripping [4,5].

With its ground state an almost pure $2s_{1/2}$ single-neutron structure [6–9] and a neutron separation energy $S_n = 1.218$ MeV, ^{15}C is a good example of a $1n$ halo. The $1n$-halo structure of ^{15}C has been investigated in several experiments at intermediate collision energies ∼ 100 MeV/u [10–12] and higher ∼1 GeV/u [7], but its influence on the low-energy reaction dynamics has been little explored to date. Only the sub-barrier ^{15}C + ^{232}Th fusion excitation function has been measured [13], the observed enhancement being irrefutably due to the halo nature of ^{15}C [14].

The near-barrier scattering of ^{15}C from a heavy target like ^{208}Pb provides an excellent system for exploring the interplay between the various possible reaction channels. Continuum Discretised Coupled Channel (CDCC) and Coupled Reaction Channel (CRC) calculations respectively predict significant coupling effects due to breakup and single-nucleon stripping when considered separately for the ^{15}C + ^{208}Pb system [15]. An important coupling effect on the sub-barrier elastic scattering and fusion due to the single-neutron stripping is also predicted by CRC calculations [16]. The strong coupling effect of the single-neutron stripping is firmly linked to the $2s_{1/2}$ configuration of the valence neutron in ^{15}C, which underlines the importance of the s-wave configuration in the formation of a neutron halo.

With the goal of disentangling the Coulomb barrier dynamics of ^{15}C, the quasi-elastic scattering of the ^{15}C + ^{208}Pb system at $E_{\rm lab} = 65$ MeV, close to the top of the Coulomb barrier, was measured at the HIE-ISOLDE facility [20], CERN. The high-granularity silicon array GLORIA [21] was used to provide a continuous angular distribution over the range $20° \leq \theta_{\rm lab} \leq 120°$.

This paper is structured as follows: Sections 2 and 3 describe the experimental setup and the data reduction procedures. Section 4 presents the results of new calculations including simultaneous coupling to breakup and single-neutron stripping. The results of the analysis are discussed in Section 5, which also includes a comparison with data for the well-known ^{12}C + ^{208}Pb scattering system at a similar collision energy [24]. Section 6 provides a summary and conclusions.

2. Experimental setup

The ^{15}C isotope was produced at ISOLDE [18] by spallation reactions induced by a 1.4 GeV proton beam on a CaO primary target. After ionisation in a plasma source, extraction and mass separation (GPS), the ^{15}C beam was bunched (REX-Trap), further ionised (EBIS [17], Q = 5+) and injected into REX [19] and HIE-ISOLDE [20] for post-acceleration to 65 MeV. The main beam contaminant was ^{15}N, originating from EBIS (residual gas), at the same kinetic energy and an intensity of 10^4 pps, which was used for beam monitoring. With a much higher Coulomb barrier, any contribution from ^{15}N induced reactions to the carbon yield can be neglected. Additional runs with ^{12}C and ^{18}O beams at the same E/A were also provided for geometry optimisation and data normalisation.

Detection of the scattered ions employed the GLORIA (Global Reaction Array) detector [21], consisting of six multi-segmented $\Delta E + E$ silicon telescopes. Each telescope comprised a 40 μm thick ΔE double-sided silicon strip detector (DSSSD) backed by a 1 mm thick DSSSD (E detector), able to stop all particles punching through the thin ΔE detector. All DSSSDs were produced by Micron Semiconductor Ltd. (model W1) [22] and comprised 16 strips on both front (X axis) and rear (Y axis) faces, providing a total of 256 pixels.

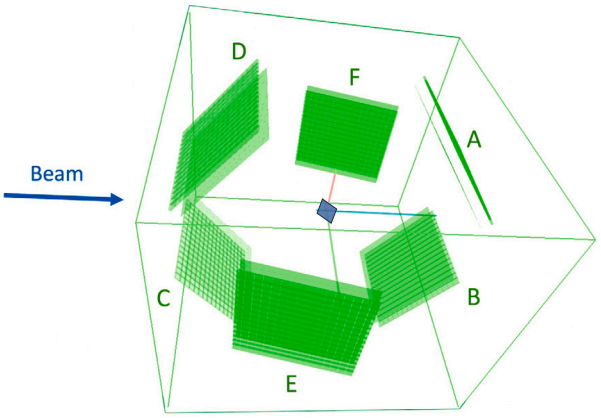

Fig. 1. 3D visualisation of the six GLORIA telescopes, labelled A to F. The target foil is shown in blue and the beam direction is indicated by the arrow.

GLORIA telescopes were placed tangentially to a 6 cm radius sphere centred on the reaction target, with a total solid angle coverage of ∼ 25% of 4π and an angular granularity of 3° per pixel. To provide a continuous angular distribution, the target ladder was oriented at 30° with respect to the beam direction. Two of the telescopes (A+B) were symmetrically placed covering forward angles ($15° \leq \theta_{\rm lab} \leq 65°$), another symmetric pair (C+D) covering backward angles ($115° \leq \theta_{\rm lab} \leq 165°$), and the two middle telescopes (F+E) were placed to avoid any shadow from the target plane, covering the angular ranges $60° \leq \theta_{\rm lab} \leq 100°$ and $80° \leq \theta_{\rm lab} \leq 120°$ respectively. An enriched ^{208}Pb target from ISOFLEX [23] of 97.85% purity was used, with a thickness of 2.1 mg/cm^2. The detector configuration is shown schematically in Fig. 1.

Each detector was calibrated strip-by-strip using a triple-α source (^{239}Pu, ^{241}Am, and ^{244}Cm) and a ^{148}Gd alpha source.

Given the windowless nature of the ΔE detectors, energy losses in the front dead layers were disregarded. Optimisation of the scattering and solid angles for all pixels in each telescope was based on the measured angular distribution of the elastically scattered ^{12}C beam at 52 MeV, which follows the Rutherford distribution. The X and Y coordinates of the beam on the target, as well as the two rotations around the X and Y axes, were treated as free variables, assuming that the beam direction was aligned precisely with the Z-axis. The Z coordinate was computed by default, in accordance with the GLORIA geometry due to inherent uncertainties in the beam intensity. The resulting angular distribution following the optimisation is detailed in Ref. [25].

With this geometrical optimisation, an average ^{15}C beam intensity of $1.1{\times}10^3$ pps at the reaction target was estimated for a total live-time of 140 h.

3. Data analysis and results

Elastic scattering events involving ^{15}C nuclei were identified by examining the ΔE vs. $\Delta E + E$ spectra, see Fig. 2. However, the overall energy resolution obtained was about 1 MeV (FWHM), which had an important effect on the mass resolution such that ^{14}C and ^{15}C could not be resolved. This was partly due to the rather large beam energy spread of about 225 keV (FWHM) caused by the stripper foil used to remove part of the beam contaminants and, more importantly, the low statistics which precluded the usual pixel-by-pixel analysis [21]. Therefore, depending on the scattering angle, ^{15}C elastic scattering events were mixed with inelastic scattering to the bound 0.74 MeV $5/2^+_1$ first excited state and ^{14}C nuclei from neutron stripping to excited states of ^{209}Pb; ^{14}C events from breakup should be excluded due to the larger energy separation.

The pixels within each telescope were grouped into angular sectors of 3° for telescopes A and B, and 4° for E and F. Telescopes D and C were excluded from the analysis due to the absence of ^{15}C events in the

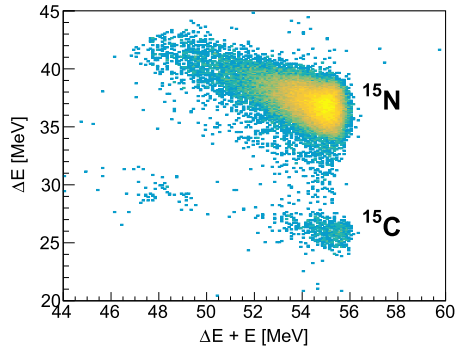

Fig. 2. Mass spectrum for the angular sector $36° \leq \theta_{lab} \leq 39°$ in telescope A. Elastically scattered ^{15}N and ^{15}C are well separated. Breakup events are observed to the left of the ^{15}C region.

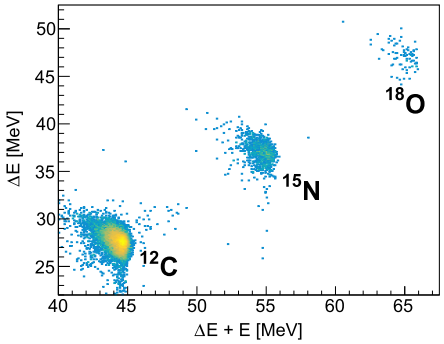

Fig. 3. Mass spectrum for the angular sector $36° \leq \theta_{lab} \leq 39°$ in telescope A with the stripper foil removed, showing elastically scattered ^{12}C, ^{15}N and ^{18}O events.

backward direction. Some pixels of telescopes A and B (forward angles) also had to be excluded due to channelling effects.

This sectorisation enhanced the clarity with which reaction channels could be identified within the mass spectra and also reduced the statistical errors. For calibration and normalisation purposes (discussed further on) a comparable methodology was applied using the ^{12}C beam (see Fig. 3).

In order to remove the uncertainties related to the detector geometry (solid angles) the ^{15}C elastic scattering yield was normalised for each angular sector using the corresponding ^{12}C yield. The ratio between the two carbon isotopes was re-normalised to 1.0 for angles within the range $20° \leq \theta_{lab} \leq 40°$ where both ^{12}C and ^{15}C exhibit pure Rutherford scattering. In order to reduce the statistical uncertainty the angular region $70° \leq \theta_{lab} \leq 120°$ was averaged over intervals of 10°.

The quasi-elastic scattering angular distribution thus obtained is compared with the elastic scattering angular distribution for 64.9 MeV ^{12}C + ^{208}Pb [24] in Fig. 4. Error bars are statistical only. Despite the uncertainties it is readily apparent that the ^{15}C + ^{208}Pb data are significantly different from the ^{12}C + ^{208}Pb elastic scattering measured at the same incident energy. The ^{15}C + ^{208}Pb data show the complete lack of a Coulomb rainbow peak associated with strong coupling effects, as predicted in Ref. [15], whereas the ^{12}C + ^{208}Pb data exhibit the usual Fresnel scattering pattern resulting from the interference of nuclear and Coulomb interactions.

4. Calculations

According to previous calculations for the ^{15}C + ^{208}Pb system at 65 MeV [15], single-neutron stripping and breakup both have a significant coupling effect on the elastic channel when considered individually. Therefore, in this work we include coupling to both processes simultaneously. All calculations were performed with the code FRESCO [26].

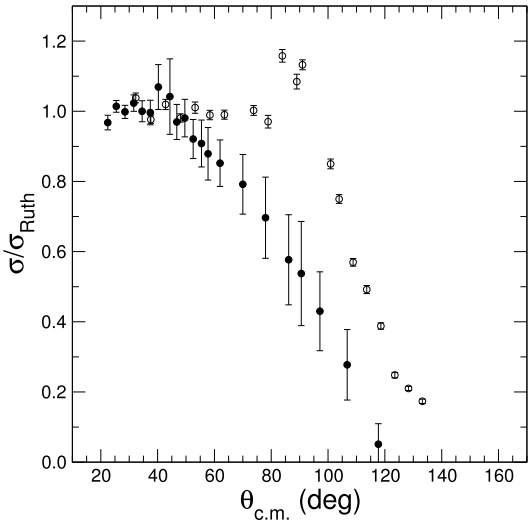

Fig. 4. Present quasi-elastic scattering data for 65 MeV ^{15}C + ^{208}Pb (filled circles) compared with the 64.9 MeV ^{12}C + ^{208}Pb elastic scattering data of Santra et al. [24] (open circles).

4.1. Breakup couplings

The $^{15}\text{C} \rightarrow n + {}^{14}\text{C}$ breakup was modelled using the CDCC formalism. A two-body cluster model of the form described in Ref. [27] was used to calculate the wave functions required as input to the CDCC calculations including couplings to the $n + {}^{14}$C continuum. The valence neutron was bound to the ^{14}C core (considered as inert) in a Woods-Saxon potential well. Since the first excited state of ^{14}C is the 6.09 MeV 1^-, the omission of core excitation should be a reasonable approximation. The parameters of the Woods-Saxon binding potential were $r_0 = 1.25$ fm, $a_0 = 0.65$ fm and a spin-orbit term of Thomas form was included with a fixed depth of 6 MeV. The depth of the central part was adjusted to reproduce the n + ^{14}C binding energy of ^{15}C. These parameters require some discussion. In addition to its ground state ^{15}C has a single bound excited state, the 0.74 MeV $5/2^+$. However, it is difficult to reconcile the adopted inelastic strength with the measured single particle strength. According to ^{14}C$(d, p)^{15}$C reaction analyses, see e.g. Murillo et al. [6] and references therein, both the ground and first excited states in ^{15}C are essentially pure single-neutron states ($C^2S \approx 1$) and should thus be well described by the $n + {}^{14}$C model. The "experimental" value of the $B(E2; 1/2^+ \rightarrow 5/2^+)$ transition in ^{15}C of 2.90 e^2fm^4 is frequently quoted in the literature, for example in Ref. [28] which gives the source as the compilation of Ajzenberg-Selove [29] where the transition rate is given as 0.44 ± 0.01 Weisskopf units (W.u.). Given the results of the (d, p) analyses one would expect the wave functions calculated using these binding potential parameters to reproduce the $B(E2; 1/2^+ \rightarrow 5/2^+)$ rather well. However, the calculated value is 0.078 e^2fm^4, almost a factor of 40 smaller than the "experimental" one. It is therefore clear that no reasonable choice of binding potential parameters will enable the $n + {}^{14}$C two-body model of ^{15}C to reproduce the "experimental" $B(E2; 1/2^+ \rightarrow 5/2^+)$. The ultimate source of the "experimental" $B(E2; 1/2^+ \rightarrow 5/2^+)$ is actually two lifetime measurements, Lowe et al. [30] and Mendelson and Carpenter [31], which give values of 3.73 ± 0.23 ns and 3.77 ± 0.11 ns respectively. It is thus possible that the usually reliable conversion of the lifetime to a transition probability may fail in this case due to the halo nature of the ^{15}C ground state. Alternatively, the simple two-body model may be inadequate to describe the wave functions, although a significant influence of core excitation seems unlikely given both the relatively large excitation energies involved and the (d, p) results. A direct determination of the transition probability via a Coulomb excitation experiment, for example, is desirable to clear up this point. In the light of the above it was decided to omit coupling to the 0.74 MeV $5/2^+$ level from the present analysis and

to retain the "standard" binding potential parameters as used in the (d, p) analysis.

Couplings to the $L = 0$, 1, 2, 3, 4, 5 and 6 non-resonant $n + {}^{14}$C continuum were included, where L denotes the angular momentum of the valence neutron relative to the ^{14}C core. The continuum was divided into a series of bins in momentum (k) space of constant width $\Delta k = 0.1$ fm^{-1} up to a maximum value of $k_{max} = 0.7$ fm^{-1}, corresponding to a maximum ^{15}C "excitation energy" of 12.19 MeV. All allowed couplings, including continuum-continuum couplings, up to multipolarity $\lambda = 6$ were included. This model space was found to give adequate convergence for both elastic scattering and breakup. Note that the same binding potential geometry is used for all "states" (including the non-resonant continuum bins) within a given calculation, in accordance with the methodology of Ref. [27].

Calculation of the diagonal and coupling potentials within this model by Watanabe-type cluster folding requires $n +$ ^{208}Pb and ^{14}C + ^{208}Pb optical model potentials at an incident energy of 4.33 MeV/nucleon. The neutron optical potential was calculated using the global nucleon parameters of Koning and Delaroche [32]. Since no suitable ^{14}C + ^{208}Pb optical potential is available the 60.9 MeV ^{12}C + ^{208}Pb potential of Santra et al. [24] was used as a surrogate. No parameters of the model were adjusted to fit the ^{15}C + ^{208}Pb quasi-elastic scattering data. A total of 700 partial waves were included in the calculation and the matching radius was set to 120 fm.

4.2. Transfer couplings

Couplings to the ^{208}Pb(^{15}C, ^{14}C)^{209}Pb single-neutron stripping reaction were included using the CRC formalism. The 69.9 MeV ^{12}C + ^{208}Pb potential of Santra et al. [24] was used as a surrogate for the exit channel ^{14}C + ^{209}Pb optical potential. The $n +$ ^{14}C binding potential was the same as used in the cluster-folding calculations for the breakup and the corresponding spectroscopic factor, $C^2S = 0.98$, is the shell model result from Table I of Ref. [33]. The $n +$ ^{208}Pb binding potential and spectroscopic factors were taken from Kovar et al. [34]. Stripping to the following states of ^{209}Pb was included: the 0.0 MeV $9/2^+$, the 1.57 MeV $5/2^+$, the 2.03 MeV $1/2^+$, the 2.49 MeV $7/2^+$, and the 2.54 MeV $3/2^+$. Transfers to the 0.78 MeV $11/2^+$ and the 1.42 MeV $15/2^-$ levels were omitted to keep the full (breakup plus stripping) calculation within tractable limits since these high spin levels are expected to make only a small contribution to both the cross section and coupling effect. Test calculations confirmed this. The post form of the interaction was used and the full complex remnant term and non-orthogonality correction were included.

5. Results and discussion

The results of the calculations are compared with the quasi-elastic scattering data in Fig. 5. As discussed previously, the data are in fact quasi-elastic scattering since they will include not only inelastic excitation of the bound $5/2^+_1$ level of ^{15}C but also ^{14}C arising from the stripping reactions; ^{14}C events resulting from breakup were separated due to the larger (and negative) Q-value. Test coupled channel calculations using the $B(E2; 1/2^+ \rightarrow 5/2^+)$ value from the literature found that omission of excitation to the ^{15}C $5/2^+_1$ level makes a negligible difference to the quasi-elastic scattering. Therefore, a calculated quasi-elastic scattering angular distribution was formed by adding the cross sections for transfer to the 2.03, 2.49 and 2.54 MeV levels of ^{209}Pb to the elastic scattering. The ^{14}C ejectiles resulting from single-neutron stripping to these levels fall within the 1 MeV energy resolution window of the quasi-elastic scattering peak. However, as shown in Fig. 5 (a), our results clearly demonstrate that although the single-neutron stripping makes a noticeable contribution to the quasi-elastic scattering for angles $\theta_{c.m.} \geq 60°$ it is within the uncertainties of the present data, which may therefore be considered as pure elastic scattering for all practical purposes.

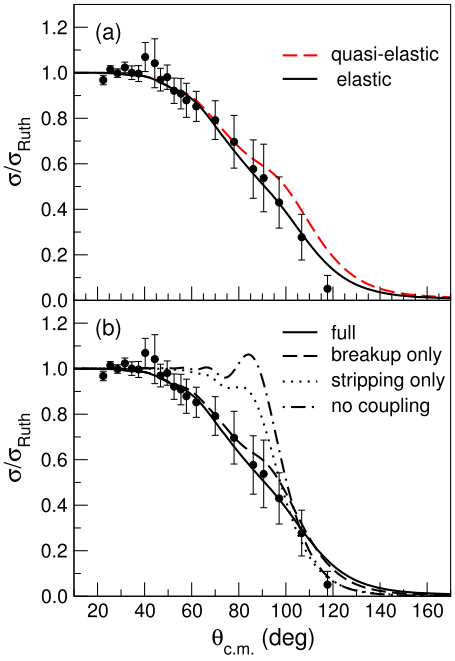

Fig. 5. Present quasi-elastic scattering data for 65 MeV ^{15}C + ^{208}Pb (filled circles) compared with the results of the calculations. (a) The quasi-elastic scattering predicted by the full (breakup + stripping coupling) calculation (dashed red curve) compared with the pure elastic scattering result (solid black curve). (b) The pure elastic scattering predicted by the full (breakup + stripping coupling) calculation (solid curve) compared with the results for breakup coupling only (dashed curve) and stripping coupling only (dotted curve). Also shown is the no coupling result (dot-dashed curve). See text for discussion.

Table 1
Total reaction cross sections (σ_R) for 65 MeV ^{15}C + ^{208}Pb and ^{12}C + ^{208}Pb [24]. The no-coupling (σ_{nc}), summed breakup (σ_{bu}) and single-neutron stripping (σ_{1n}) cross sections for the ^{15}C + ^{208}Pb system are also given. The ^{15}C + ^{208}Pb cross sections are the results of the full calculation described in the text while the ^{12}C + ^{208}Pb σ_R was derived from an optical model fit to the elastic scattering data.

System	σ_R (mb)	σ_{nc} (mb)	σ_{bu} (mb)	σ_{1n} (mb)
^{15}C + ^{208}Pb	1695	714	528	192
^{12}C + ^{208}Pb	429	—	—	—

The full calculation including both breakup and single-neutron stripping couplings is in excellent agreement with the data, although given the large uncertainties the data do not provide a rigorous test of the model. Nevertheless, they are sufficient to confirm the general prediction that these couplings completely erase the Coulomb rainbow observed in the kinematically analogous non-halo scattering system ^{12}C + ^{208}Pb [24], and in the no-coupling CRC calculations shown in Fig. 5 (b) (dot-dashed line).

The total reaction cross section and the integrated breakup and single-neutron stripping cross sections are given in Table 1. The total reaction cross section derived from the optical model fit of Santra et al. [24] for ^{12}C + ^{208}Pb elastic scattering data is also given for comparison.

Our analysis reveals the total reaction cross section for the ^{15}C + ^{208}Pb system to be almost a factor of 4 larger than that for the non-halo ^{12}C + ^{208}Pb scattering system at a similar incident energy. Indeed, the summed breakup cross section alone is some 20% larger than the ^{12}C + ^{208}Pb total reaction cross section. In addition, since the Q value for the ^{208}Pb(^{12}C, ^{11}C)^{209}Pb single-neutron stripping is −14.78 MeV and it is thus poorly matched, the large single-neutron stripping cross section for the ^{15}C + ^{208}Pb system is also significant. However, even after both

the summed breakup and single-neutron stripping cross sections have been subtracted from the total reaction cross section for ^{15}C + ^{208}Pb the remainder is still a factor of two larger than the non-halo scattering value. Much of this excess may be ascribed to the "static" effect of the halo nature of the ^{15}C ground state on the cluster-folding bare potential for ^{15}C + ^{208}Pb. This is reflected in the significantly larger reaction cross section for the ^{15}C + ^{208}Pb no coupling case compared to the ^{12}C + ^{208}Pb optical model value; the increase is almost a factor of 1.7. The residual difference provides an illustration of a common phenomenon: due to the coherent interference of reaction amplitudes, the effect of coupling to a given set of channels on the elastic scattering as evinced by the increase in the total reaction cross section is frequently larger than the sum of the separate cross sections for populating those channels. In this case the increase in the total reaction cross section due to breakup and stripping channels (981 mb), is approximately 40% larger than the addition of the individual cross sections (720 mb).

In Fig. 5 (b) we also compare the elastic scattering predicted by the full (breakup + stripping) calculation with that predicted by coupling to breakup only and stripping only. It is readily apparent that while the effect of the stripping coupling by itself is significant—it leaves only a slight hint of the Coulomb rainbow observed in the no coupling result—the influence of the breakup coupling is dominant. It is however noteworthy that in the angular range around the Coulomb rainbow peak (in the no-coupling angular distribution) the coupling effect of the stripping when combined with breakup is significantly reduced compared to that found when just the stripping coupling is present, cf. the difference between the solid and dashed curves versus that between the dotted and dot-dashed curves on Fig. 5 (b). This non-linearity of coupling effects when combining different couplings even when their only interaction is via their influence on the entrance channel is also frequently observed.

6. Summary and conclusions

The near-barrier elastic scattering of ^{15}C from a heavy target (^{208}Pb) was measured for the first time. Despite difficulties associated with low beam current on target, the quasi-elastic scattering angular distribution was obtained, albeit with relatively large uncertainties due to the poor statistics. The precision was nevertheless sufficient to confirm the large coupling effects predicted for this system [15]. While the coupling influence due to the ^{208}Pb(^{15}C, ^{14}C)^{209}Pb single-neutron stripping is significant, the overall effect is dominated by the $^{15}\mathrm{C} \rightarrow n + {}^{14}\mathrm{C}$ breakup.

A two-body $n + {}^{14}$C model is able satisfactorily to describe the quasi-elastic scattering data within the obtained precision when implemented within the CDCC formalism. However, the model fails to reproduce the "experimental" $B(E2; 1/2^+ \rightarrow 5/2^+)$ for excitation of the bound 0.74 MeV $5/2^+$ level of ^{15}C, underpredicting it by a large factor, in spite of both the ground and 0.74 MeV states being almost pure single neutron levels according to the results of ^{14}C(d, p)^{15}C analyses [6]. This apparent paradox could be linked to the "experimental" $B(E2)$ being in fact derived from lifetime measurements [30,31]; it is possible that the halo nature of the ^{15}C ground state may affect the usually reliable conversion of a lifetime to a transition strength. A more direct measurement of the strength, via a Coulomb excitation experiment, for example, is desirable to clear up this point. If the currently accepted value of the $B(E2; 1/2^+ \rightarrow 5/2^+)$ is indeed found to be accurate it would point to a more complex structure for either or both of these levels than has hitherto been assumed.

The total reaction cross section for ^{15}C + ^{208}Pb at 65 MeV is approximately a factor of four greater than that for ^{12}C + ^{208}Pb at the same energy (cf. Table 1). This is linked to the contributions from breakup and single-neutron stripping, absent for ^{12}C, although some of the increase may be ascribed to "static" effects due to the influence of the halo nature of the ^{15}C ground state on the ^{15}C + ^{208}Pb bare potential calculated using the two-body cluster-folding model, cf. the total reaction cross sections for ^{12}C + ^{208}Pb and the no coupling ^{15}C + ^{208}Pb case in Table 1. The bulk of the increase is, however, attributable to the dynamic coupling effects.

In summary, the present data are consistent with the picture of ^{15}C as a neutron halo nucleus, in spite of the relatively high S_n value of 1.2 MeV. This appears to be due to the essentially pure $2s_{1/2}$ structure of the ground state, which is also responsible for the large single-neutron stripping. The significance of the dynamic effects of breakup (dominant) and neutron stripping, together with the static effect on the bare potential of the halo nature of the ground state, explain the important difference between the near-barrier elastic scattering of ^{15}C + ^{208}Pb from that of ^{12}C + ^{208}Pb at the same incident energy, with the dynamic effects from coupling dominating.

This work was partially funded by the grants DFF–4181-00218 of the Danish Council for Independent Research, CONACYT315839, DGAPA-PAPIIT IG101423 of the Mexican Government, PGC2018-095640-B-I00, PID2021-1269980-B-I00, PGC2018-095640-B-I00, RTI2018-098868-B-I00, PID2022-140162NB-I00, "Unidad Asociada GIFMAN–CSIC-UHU" of the Spanish funding agency MCIN-AEI DOI10.13039 -501100011033 (FEDER, EU), and the European Union's Horizon 2020 research and innovation programme under grant agreement no. 654002 (ENSAR2). One of us (V. G. Távora) would also like to acknowledge the financial support received from the grant PID2019-104390 GB-I00 of the Spanish Government.

Declaration of competing interest

The authors declare that they have no known competing financial interests or personal relationships that could have appeared to influence the work reported in this paper.

Data availability

Data will be made available on request.

References

[1] I. Tanihata, et al., Phys. Rev. Lett. 55 (24) (1985) 2676.
[2] K. Riisager, Phys. Scr. T 152 (2013) 014001.
[3] I. Martel, EPJ Web Conf. 252 (2021) 04003.
[4] N. Keeley, N. Alamanos, K.W. Kemper, K. Rusek, Prog. Part. Nucl. Phys. 63 (2009) 396.
[5] J.J. Kolata, V. Guimaraes, E.F. Aguilera, Eur. Phys. J. A 52 (2016) 123.
[6] G. Murillo, S. Sen, S.E. Darden, Nucl. Phys. A 579 (1994) 125.
[7] A. Ozawa, et al., Nucl. Phys. A 691 (2001) 599.
[8] J.R. Terry, et al., Phys. Rev. C 69 (2004) 054306.
[9] S. Truong, H.T. Fortune, Phys. Rev. C 28 (1983) 977.
[10] D. Bazin, et al., Phys. Rev. C 57 (1998) 2156.
[11] E. Sauvan, et al., Phys. Lett. B 491 (2000) 1.
[12] D.Q. Fang, et al., Phys. Rev. C 69 (2004) 034613.
[13] M. Alcorta, et al., Phys. Rev. Lett. 106 (2011) 172701.
[14] Xiang-Xiang Sun, Lu Guo, Phys. Rev. C 107 (2023) L011601.
[15] N. Keeley, K.W. Kemper, K. Rusek, Eur. Phys. J. A 50 (2014) 145.
[16] N. Keeley, N. Alamanos, Phys. Rev. C 75 (2007) 054610.
[17] B.H. Wolf, et al., Nucl. Instrum. Methods Phys. Res. B 204 (2003) 428.
[18] E. Kugler, Hyperfine Interact. 129 (2000) 23.
[19] D. Habs, O. Kester, T. Sieber, et al., Hyperfine Interact. 129 (2000) 43–66.
[20] https://hie-isolde-project.web.cern.ch.
[21] G. Marquínez-Durán, et al., Nucl. Instrum. Methods A 755 (69) (2014).
[22] https://www.micronsemiconductor.co.uk.
[23] https://www.isoflex.com.
[24] S. Santra, et al., Phys. Rev. C 64 (2001) 024602.
[25] V.G. Távora, et al., EPJ Web Conf. 290 (2023) 02005.
[26] I.J. Thompson, Comput. Phys. Rep. 7 (1988) 167.
[27] B. Buck, A.A. Pilt, Nucl. Phys. A 280 (1977) 133.
[28] C.A. Bertulani, et al., Phys. Lett. B 650 (1997) 233.
[29] F. Ajzenberg-Selove, Nucl. Phys. A 523 (1991) 1.
[30] J. Lowe, C.L. McClelland, J.V. Kane, Phys. Rev. 126 (1962) 1811.
[31] R.A. Mendelson Jr., R.T. Carpenter, Phys. Rev. 166 (1968) 988.
[32] A.J. Koning, J.P. Delaroche, Nucl. Phys. A 713 (2003) 231.
[33] M.B. Tsang, J. Lee, W.G. Lynch, Phys. Rev. Lett. 95 (2005) 222501.
[34] D.G. Kovar, N. Stein, C.K. Bockelman, Nucl. Phys. A 231 (1974) 266.